INTERNATIONAL JOURNAL FOR NUMERICAL AND ANALYTICAL METHODS IN GEOMECHANICS
Int. J. Numer. Anal. Meth. Geomech., 2003; **27**:603–626 (DOI: 10.1002/nag.288)

Glyph and hyperstreamline representation of stress and strain tensors and material constitutive response

Youssef M. A. Hashash[1,*,†,‡], John I-Chiang Yao[2,§] and Donald C. Wotring[2,§]

[1] *Department of Civil and Environmental Engineering, University of Illinois at Urbana-Champaign, RM 2230C NCEL, 205 N. Mathews Ave. Urbana, Illinois 61801, USA*

[2] *Department of Civil and Environmental Engineering, University of Illinois at Urbana-Champaign, USA*

SUMMARY

Results of numerical analyses of boundary value problems in geomechanics include output of three-dimensional stress and strain states. Two-dimensional plots of stress–stress or stress–strain quantities, often used to represent such output, do not fully communicate the evolution of stress and strain states. This paper describes the use of glyphs and hyperstreamlines for the visual representation of three dimensional stress and strain tensors in geomechanics applications. Glyphs can be used to represent principal stress states as well as normal stresses at a point. The application of these glyphs is extended in this paper to represent strain states. The paper introduces a new glyph, called HWY glyph for the representation of shear tensor components. A load step-based hyperstreamline is developed to show the evolution of a stress or strain tensor under a general state of loading. The evolution of stress–strain states from simulated laboratory tests and a general boundary value problem of a deep braced excavation are represented using these advanced visual techniques. These visual representations facilitate the understanding of complex multidimensional stress–strain soil constitutive relationships. The visual objects introduced in this paper can be applied to stress and strain tensors from general boundary value problems. Copyright © 2003 John Wiley & Sons, Ltd.

KEY WORDS: constitutive relations; soil models; plasticity; hyperstreamlines; glyphs; stress tensor; strain tensor; visualization

INTRODUCTION

Visual representation of stress and strain response in three-dimensional space plays a crucial role in post-processing and data analysis for large-scale finite element model simulations of physical problems including those encountered in geotechnical engineering. The large quantity of output (material or integration) points from 2-D finite element models or 3-D models can

*Correspondence to: Youssef M.A. Hashash, Department of Civil and Environmental Engineering, University of Illinois at Urbana-Champaign, RM 2230C NCEL, 205 N. Mathews Ave. Urbana, Illinois 61801, USA
† E-mail: hashash@uiuc.edu
‡ Assistant Professor
§ Graduate Research Assistant

Contrat/grant sponsor: National Science Foundation; contract/grant number: CMS 99-84125.

Received 30 October 2002
Revised 4 February 2003

easily overwhelm the traditional method of displaying variables in 2-D plots. Often, each output point includes multiple variables that contain characteristics of interest to the analyst. The problem becomes even more difficult if the analyst needs to examine the evolution of variables such as stresses and strains with change in loading conditions. Effective and intuitive representation of output results is as important as model development and analysis execution.

Hashash *et al.* [1] introduce a novel interactive visualization development and learning environment for material constitutive relations, VizCoRe (visualization of constitutive relations). The objective of VizCoRe is to transform the representation of constitutive relations, as well as stress and strain quantities from a series of mathematical equations and matrix quantities to multi-dimensional geometric/visual objects in a dynamic interactive colour-rich display environment.

This paper describes the original development and use, within VizCoRe, of 3-D visual objects called glyphs and hyperstreamlines to represent stress and strain tensors. The usefulness and limitations of these glyphs are demonstrated using stress and strain paths from geotechnical laboratory tests and a braced excavation boundary value problem. The proposed 3-D objects complement 2-D plots used to represent states of stress and strain (e.g. Mohr's circle, and p-q stress paths).

Advances in computer hardware and software technologies make the use of the proposed objects accessible to most users of numerical analysis. In this paper the 3-D objects are printed on a 2-D surface, however, they are best used interactively on a computer terminal. The figures presented in the hard copy version of this paper use grey scale while the online version figures are in colour. Some of the figures are displayed using wire frames while others are shown using solid surfaces to enhance the clarity of presentation.

GLYPHS AND HYPERSTREAMLINE REPRESENTATION OF SECOND ORDER STRESS AND STRAIN TENSORS

A glyph, in the parlance of visualization, is a geometric icon that represents multi-variate or higher-dimensional information at a given position [2]. Physical properties of a glyph are affected by the input data. The colour, size and geometry vary based on scalar values. The orientation in space depends on a vector quantity. The geometry of a glyph can be developed using one of two methods:

1. *Manipulation of a predefined geometric object*: This method requires that the geometry of a predefined object changes with some scalar and/or vector quantities. For example, an arrow at a particular position within a flow field is oriented along the direction of flow, a vector quantity, and could be sized dependent on the magnitude of flow, a scalar value.
2. *Direct inheritance of physical properties from formulation*(*s*): In this method, glyphs that are constructed based on formulation(s) directly related to the property of interest. The shape of the glyph is not pre-defined, but is described completely by the formulation(s).

A Hyperstreamline is a continuous geometric structure that can be extracted from a tensor field [3,4]. It is used to emphasize continuous changes in tensor properties. Physical properties of a hyperstreamline include those of a glyph as well as trajectory in space that depends on a vector

quantity to describe the change in the tensor quantity. Hyperstreamlines are further characterized by the geometry of their cross-section [4]:

1. A series of connected ellipses generate a hyperstreamline called a tube. This type of hyperstreamline is used in this paper.
2. A series of connected crosses generate a hyperstreamline called a helix.

Glyphs provide an instantaneous representation of a tensor quantity, while hyperstreamlines show the evolution of the tensor quantity. A glyph has to be animated to examine the change in a tensor quantity. Although glyphs and hyperstreamline are applied to represent stress and strain data in this paper, they can represent any 3-D tensor field.

Glyphs and hyperstreamline techniques have rarely been used to represent stress and strain states and constitutive relations in geomechanics (Jeremic *et al.* [5]). They provide graphically new insights into many engineering problems. Under the most general loading condition, a state of stress at a point is represented by a second order stress tensor (σ_{ij}) with nine scalar stress components. Similarly, a state of strain can be represented by a second order strain tensor (ε_{ij}) as illustrated in Figure 1. Symmetry of the stress and strain tensors (i.e. no rigid body rotation) reduces the number of independent components in each tensor to six.

Glyphs can be used to represent 2nd order stress or strain tensor data. One of the earliest and most common representations of a second order stress tensor is the stress quadric described by Frederick and Chang [6]. Several more recent works have been published to graphically examine second order symmetric stress tensors using techniques such as glyphs [7] and hyperstreamlines [8,4]. The choice of glyphs for visual representation depends on the property of interest. In many cases, multiple glyph types may be needed to capture all of the properties that are relevant to a problem. Five glyph types are introduced in this paper: (1) Lamé stress ellipsoid [9], (2) Haber [2], (3) Cauchy's stress quadric [9], (4) Reynolds [7], and (5) HWY, developed by the authors in this paper. The Lamé and Haber glyphs are used to visualize principal stress states, while the Cauchy's stress quadric and the Reynolds glyph show the normal stress acting on a point in any direction. The paper extends the use of these glyphs to represent strain

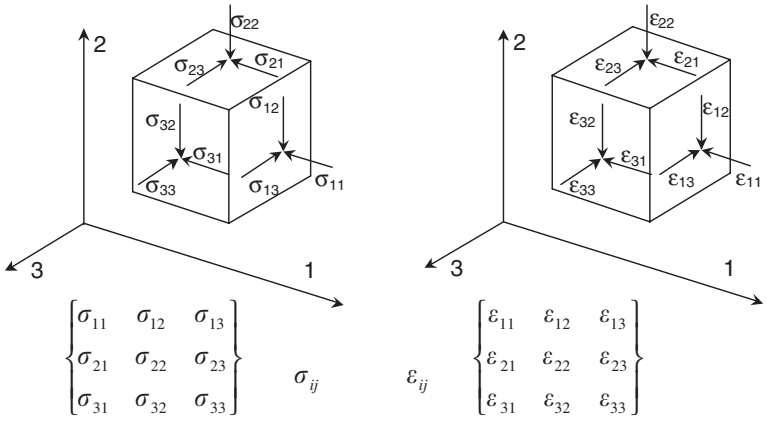

$$\sigma_{ij} = \begin{Bmatrix} \sigma_{11} & \sigma_{12} & \sigma_{13} \\ \sigma_{21} & \sigma_{22} & \sigma_{23} \\ \sigma_{31} & \sigma_{32} & \sigma_{33} \end{Bmatrix} \qquad \varepsilon_{ij} = \begin{Bmatrix} \varepsilon_{11} & \varepsilon_{12} & \varepsilon_{13} \\ \varepsilon_{21} & \varepsilon_{22} & \varepsilon_{23} \\ \varepsilon_{31} & \varepsilon_{32} & \varepsilon_{33} \end{Bmatrix}$$

Figure 1. Stress and strain tensors at a point.

states. The paper introduces a load-step based hyperstreamline to plot stress and strain histories. Table I summarizes the features of glyphs and hyperstreamlines presented in this paper.

Glyphs for representation of principal stress state

The problem of visualizing the six independent stress components is replaced by representing three orthogonal vectors whose magnitude is equal to the eigenvalue of the second order tensor and whose direction is defined by the corresponding eigenvector. The second order stress tensor in Figure 1 can be transformed into an eigenvalue–eigenvector problem as shown in the following formulation:

$$\begin{vmatrix} \sigma_{11}-\sigma & \sigma_{12} & \sigma_{13} \\ \sigma_{21} & \sigma_{22}-\sigma & \sigma_{23} \\ \sigma_{31} & \sigma_{32} & \sigma_{33}-\sigma \end{vmatrix} = 0 \tag{1}$$

The magnitudes of the principal stresses (eigenvalues) can be determined by expanding the determinate in Equation (1) and solving variable σ for the three roots, σ_a, σ_b, and σ_c. The principal stress directions (eigenvectors) can be found by substituting each of the principal stresses (σ_a, σ_b, σ_c) into Equation (2) and solving for the components of the column vector (m_a, m_b, m_c).

$$\begin{bmatrix} \sigma_{11}-\sigma & \sigma_{12} & \sigma_{13} \\ \sigma_{21} & \sigma_{22}-\sigma & \sigma_{23} \\ \sigma_{31} & \sigma_{32} & \sigma_{33}-\sigma \end{bmatrix} \begin{bmatrix} m_a \\ m_b \\ m_c \end{bmatrix} = 0 \tag{2}$$

The cube shown in Figure 2 illustrates the orientation of the principal stress and can be considered as a crude glyph oriented in the principal stress directions. The shapes of the Lamé stress ellipsoid and the Haber glyph can more clearly represent the magnitude and orientation of the principal stresses.

Lamé stress ellipsoid glyph. The concept of the stress ellipsoid was noted by Cauchy and by Lamé during the period of founding of the theory of elasticity between 1820 and 1830 [9]. Lamé stress ellipsoid is a glyph with its three axes defined by the absolute magnitudes of the major, intermediate and minor principal stresses represented by σ_a, σ_b, and σ_c, respectively (Figure 3). The following equation describes the geometry of the elliposid:

$$\frac{(x_a)^2}{(\sigma_a)^2}+\frac{(x_b)^2}{(\sigma_b)^2}+\frac{(x_c)^2}{(\sigma_c)^2}=1 \tag{3}$$

where x_a, x_b and x_c are variables along the major, intermediate and minor principal axes respectively shown in Figure 2. Under an isotropic state of stress, the glyph is a sphere.

Figure 3 shows the Lamé stress ellipsoid in stress space under various stress states. The glyphs are oriented in the principal stress directions. The geometry of the Lamé stress ellipsoid alone cannot indicate the signs of the principal stresses. In this paper, the glyph is improved by colour-mapping the surface of the ellipsoid based on the magnitude of the major principal stress. This is accomplished by taking all of the calculated major principal stresses throughout the entire load history and assigning the values to a predefined RGB (Red, Green, Blue) colour or grey scale, whereby the warmer (e.g. red) colours or lighter shades represent higher stresses (compression is

Table I. Advantages and limitations of glyph and hyperstreamline representations.

	Display features	Advantages	Limitations
Lamé stress ellipsoid glyph	Orientations and magnitudes of principal stresses & strains	Isotropic state is a sphere	Difficult to see principal directions for nearly isotropic states
Haber Glyph	Orientations and magnitudes of principal stresses & strains	Clearly represents orientation even for nearly isotropic states Represents magnitudes and signs of all principal values using colour mapping	Difficult to identify K_0 condition when $K_0 > 1.0$
Cauchy stress Glyph	Normal stress/strain components	Represents magnitude of normal stress/strain in any direction Shows the magnitudes and orientations of the principal stresses/strains Isotropic state is a sphere	The shape is not intuitive since magnitude of the normal stress/strain is inversely proportional to the square of the size
Reynolds Glyph	Normal stress/strain components	Clearly represents magnitudes of normal stress/strain in any direction Shows the magnitudes and orientations of principal components Isotropic state is a sphere	Difficult to see principal directions for nearly isotropic states
HWY Glyph	Magnitude of stress/strain shear component	Clearly represents magnitudes of shear stress/strain on any plane Shows the orientations of principal components Isotropic state of stress results in nill glyph	Does not show orientation of shear components
Load history Hyperstreamline	Magnitude and orientation of principal stress/strain history	Represents loading history in a single display Useful to compare response from different constitutive models.	Cannot indicate the sign for all principal components. Difficult to identify $K_0 > 1.0$ condition.

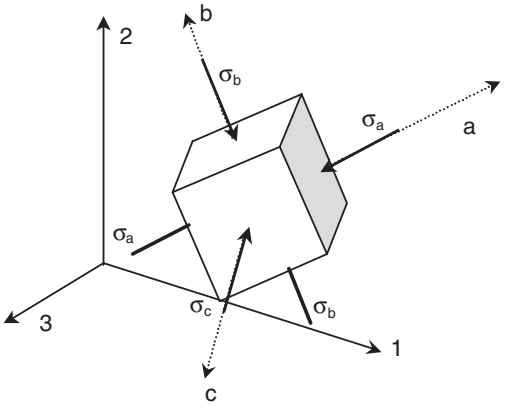

Figure 2. Principal stress state, eigenvalues and eigenvector, corresponding to the general state of stress in Figure 1.

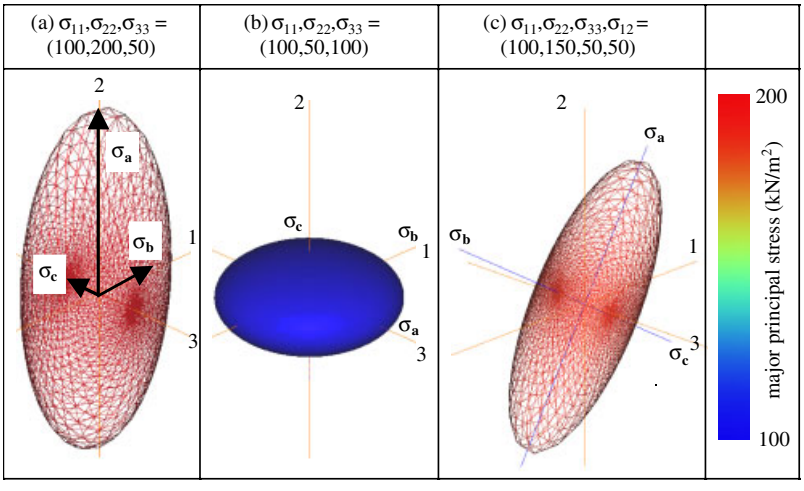

Figure 3. Lamé stress ellipsoid glyph (stress components not given are equal to zero).

positive) and the cooler (e.g. blue) colours or darker shades indicate lower stresses. For example, the colour would be blue at the step of the load history where the major principal stress is at its minimum. The colour-mapping scheme offers the ability to not only show the sign of the current major principal stress, but also its magnitude relative to stresses at other loading steps.

Figure 3(a) shows a state of stress whereby the principal stresses are aligned with axes of the reference frame. The glyph is an ellipsoid. Figure 3(b) shows a state of stress with $K_0 > 1.0$ resulting in a glyph that is axisymmetric about the 2-axis. In Figure 3(c), where a shear stress is introduced, the glyph principal axes are rotated relative to the reference frame.

Haber glyph. Haber [2] developed a principal stress glyph and used clusters of these glyphs as visual aids in the study of the singular stresses around propagating cracks. The geometry of the

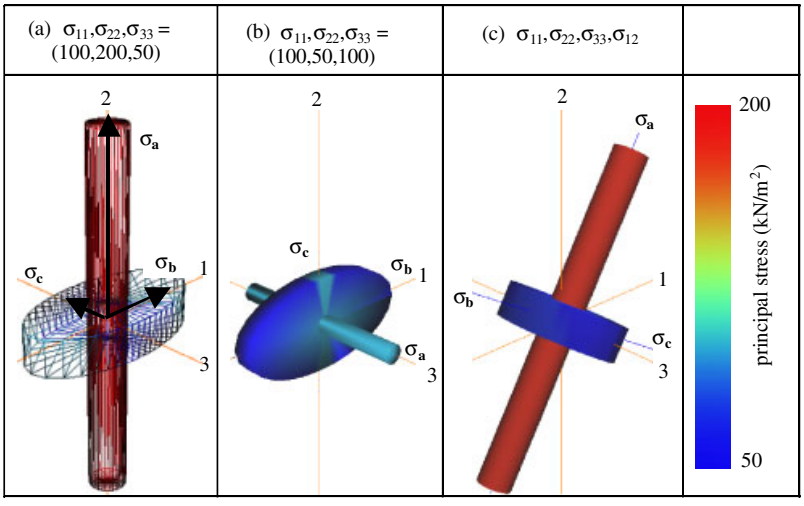

Figure 4. Haber stress glyph (stress components not given are equal to zero).

Haber glyph is illustrated in Figure 4. The half-length of the cylindrical rod represents the magnitude of the major principal stress (σ_a), and the shape of the elliptical disk is controlled by the magnitudes of the intermediate (σ_b) and minor (σ_c) principal stresses. The disk is circular when the intermediate and minor principal stresses are equal such as in a conventional laboratory triaxial test. The dimensions of the disk are scaled relative to the shaft length, by a factor α. Haber [2] used a value of $\alpha = 2$ to make it easier to see the disk when the magnitude of the major principal stress dominates the other principal stresses. However, $\alpha = 1$ is more suitable for stress states in geotechnical applications. Colour/greyscale-mapping is applied to the surface of the shaft and disk to indicate the signs and values of the principal stresses. This is achieved by taking all of the principal stresses throughout the entire load history and assigning the values to an RGB colour scale (or grey scale). As a result, the maximum value on the scale represented by the colour red (lighter shade) is the largest major principal stress, while the minimum value indicated by the colour blue (darker shade) is the smallest minor principal stress in the load history. Two different colours are mapped onto the elliptical disk. The colouring scheme divides the disk equally (in degrees) into four areas. The colour on one set of areas along the longer axis of the disk shows the magnitude of the intermediate principal stress, while the colour on the other set along the narrower axis indicates the minor principal stress. A grey scale scheme (see Lamé Stress Ellipsoid Glyph) can be used instead of the RGB colour scheme. Principal stress directions define the glyph's orientation.

The Haber glyph does not clearly represent K_0 states of stress when K_0 is greater than unity (Figure 4(b)). Under triaxial loading, if the horizontal stresses are greater than vertical, Haber's glyph will represent one of the horizontal stresses as its shaft and the other horizontal stress and the vertical stress as the disk. It is difficult for the viewer to immediately recognize that the sample is under K_0 state of stress without knowledge of the test or stress values. In such cases, Lamé stress ellipsoid is a more suitable glyph (compare Figure 3(b) and Figure 4(b)). The Haber glyph clearly shows the orientation of principal stress axes (Figure 4(c)).

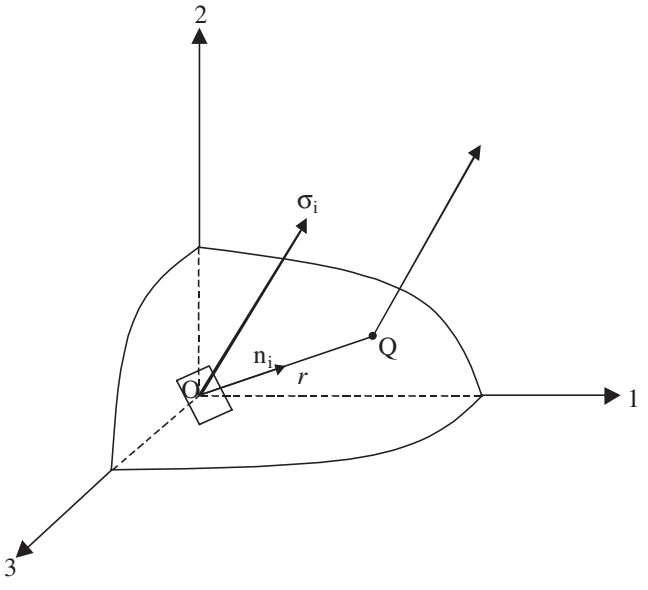

Figure 5. Schematic of a stress quadric (after Frederick and Chang [6]).

Glyphs for representation of normal stresses

Cauchy's stress quadric glyph (stress quadric). If the stress tensor at a point O, Figure 5, is σ_{ij}, then the following represents a quadric surface with its centre at O (after Frederick and Chang [6]):

$$\sigma_{ij}x_i x_j = \sigma_{11}x_1^2 + \sigma_{22}x_2^2 + \sigma_{33}x_3^2 + 2\sigma_{23}x_2x_3 + 2\sigma_{31}x_3x_1 + 2\sigma_{12}x_1x_2 = \pm k^2 \tag{4}$$

where x_i are the co-ordinates of the points on the surface, and k is a constant.

Frederick and Chang describe two relevant properties of the stress quadric:

1. Let Q be a point on the quadric surface, and let the distance OQ $= r$ (Figure 5). Then the normal stress at O, acting across the surface normal to OQ, is inversely proportional to r^2.

$$\sigma_N = \sigma_{ij}n_i n_j = \sigma_{ij}\left(\frac{x_i}{r}\right)\left(\frac{x_j}{r}\right) = \pm\frac{k^2}{r^2} \quad \text{or } r = \sqrt{\left|\frac{k^2}{\sigma_N}\right|} \tag{5}$$

   where σ_N is the normal stress at O corresponding to the direction of OQ, and n_i direction cosines of a unit vector corresponding to the direction of OQ.
2. The stress vector σ_i at O, acting across the area that is normal to OQ, is parallel to the normal to the surface of the stress quadric at Q.

Colours (or grey scale) are mapped on the surface to give relative magnitudes and sign of the normal stress using the procedure described for previous glyphs.

Figure 6 illustrates the stress quadric under different stress states. Based on the first property of the stress quadric (Equation (5)), the largest normal stress is represented by the shortest radius (r_{nA}) from the origin to the surface of the stress quadric and *vice versa* for the smallest normal stress represented by r_{nB} (Figure 6(a)). The glyph is naturally oriented in the principal

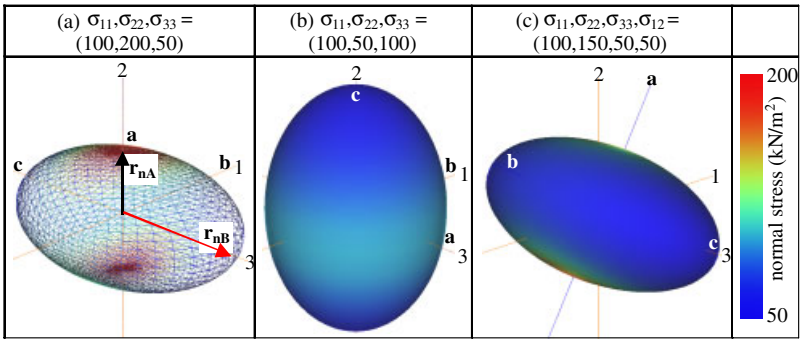

Figure 6. Cauchy's stress quadric glyph (stress components not given are equal to zero).

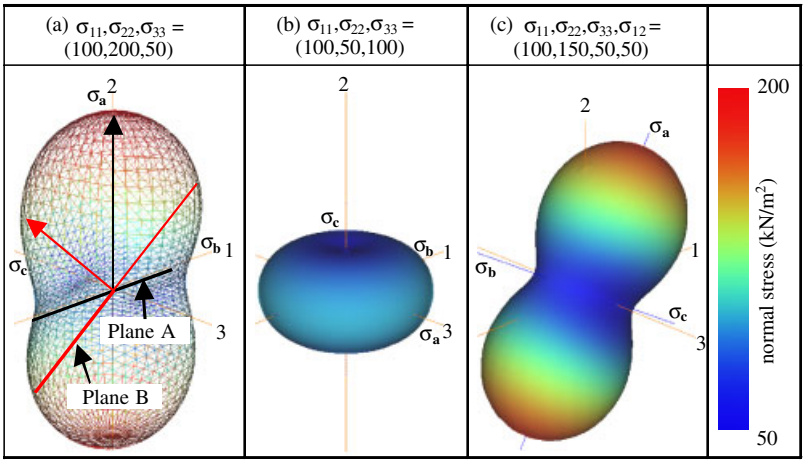

Figure 7. Reynolds stress glyph (stress components not given are equal to zero).

directions (Figure 6(c)). However, the geometry of the quadric is not intuitive since the size of the glyph is inversely proportional to the square root of the magnitude of the normal stress.

Reynolds stress glyph. Moore *et al.* [10] proposed a solid surface model (or 3-D glyph), the Reynold stress glyph, to gain insights from turbulence and stress measurements in 3-D flows. The Reynolds glyph surface is defined such that the distance from the origin of the glyph to any point on its surface is the magnitude of normal stress in that direction. The normal stress (σ_N) in any direction can be determined using the following equation:

$$\sigma_N = \sigma_{ij} n_i n_j \tag{6}$$

where (n_1, n_2, n_3) are the direction cosines of a unit vector that is perpendicular to the plane of interest. Therefore, the magnitude of the normal stress is directly proportional to the size of the glyph. Figure 7 presents examples of Reynolds glyph whereby colours (or varying shades of grey) are mapped on the surface in the same way as the stress quadric to give relative magnitudes and sign of the normal stress. Under isotropic state of stress, the glyph is a sphere. By introducing a shear stress, Figure 7(c), the glyph rotates off of the reference co-ordinate

system. The surface of the Reynolds glyph is defined such that the distance from the origin of the glyph to any point on its surface is the magnitude of the normal stress in that direction, therefore, the glyph would naturally rotate itself in the principal stress directions such that its long and narrow axes align with the major and minor principal stress directions, respectively. Hence, the Reynolds glyph can be utilized as a principal stress glyph.

Using the Reynolds stress glyph is similar to using a Mohr's circle. The state of stress of $[\sigma_{11}, \sigma_{22}, \sigma_{33}] = [100, 200, 50]$ shown in Figure 7(a) is illustrated in more detail in Figure 8(a) with a corresponding Mohr circle representation of state of stress in 1–2 plane, Figure 8(c). Using the Mohr circle (see Figure 8(c)) the magnitude of stress on any arbitrary plane is found by drawing a line from the pole in the orientation that is parallel to the plane of interest. The magnitudes of normal and shear stresses acting on the plane are indicated at the point where the line crosses the Mohr's circle (e.g. planes A and B). In the Reynolds glyph a line from the origin of axes oriented

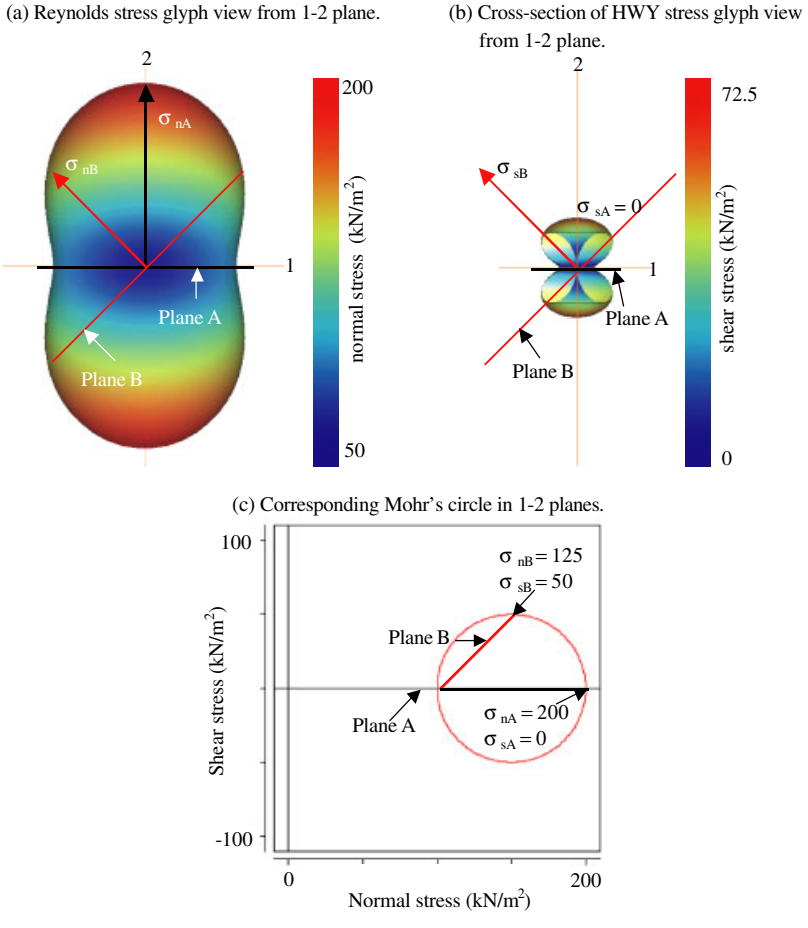

Figure 8. Reynolds and HWY stress glyphs and Mohr circle, $\sigma_{11} = 100$ & $\sigma_{22} = 200$; (a) Reynolds stress glyph view from 1–2 plane; (b) Cross-section of HWY stress glyph view from 1–2 plane; (c) Corresponding Mohr's circle in 1–2 planes.

normal to the plane of interest intersects the glyph at a point whose distance from the origin is equal to the normal stress on that plane. The Reynolds glyph does not provide the value of the shear stress acting on a plane.

Glyph for representation of shear stresses, HWY shear glyph

A new type of glyph named 'HWY' is introduced to visualize the shear stress magnitude on any arbitrary plane. The name of the glyph represents alphabetically the initials of the authors. The HWY glyph is similar to the Reynolds glyph. Since a stress vector (T) on an arbitrary plane can be separated into a normal (Equation (6)) and a shear stress component (σ_S), the magnitude of the shear stress can be computed as

$$\sigma_S = \sqrt{T^2 - \sigma_N^2} = \sqrt{T_i T_i - \sigma_N^2} \quad \text{where } T_i = \sigma_{ij} n_j \tag{7}$$

The surface of the HWY glyph can be defined such that the length of a line drawn from the origin of the glyph to a point on its surface represents the magnitude of the shear stress, σ_S, acting in a plane perpendicular to that line (similar to determining the magnitude of the normal stresses in the Reynolds glyph). The glyph does not provide the direction of the shear stress in that plane.

Under isotropic state of stress, the glyph is a point at zero. Examples of the three-dimensional HWY glyph shown in Figure 9 can be used to visualize the shear stress on any plane. A colour map or grey scale is used to represent the magnitude of the shear stress on the glyph surface. By introducing a shear stress component in the 1–2 plane, Figure 9(c), the glyph rotates off of the reference co-ordinate system along principal directions similar to the Reynolds glyph.

Figure 8(b) shows a HWY glyph in the 1–2 plane corresponding to a state of stress of $[\sigma_{11}, \sigma_{22}, \sigma_{33}] = [100, 200, 50]$. Figure 9(a) shows a wire-frame view of the same HWY glyph from a different viewing angle, with the left petal tracing the glyph in the 1–2 plane. The HWY shear glyph can be used similar to the Reynolds glyph to determine the magnitude of the shear stress on a plane. In the 1–2 plane, the shear stress increases with the slope of the plane until it reaches maximum on Plane B (at 45° to the horizontal 1-axis) and gradually drops back to zero as the slope of the plane reduces to zero on Plane A. This is similar to the result one would get tracing

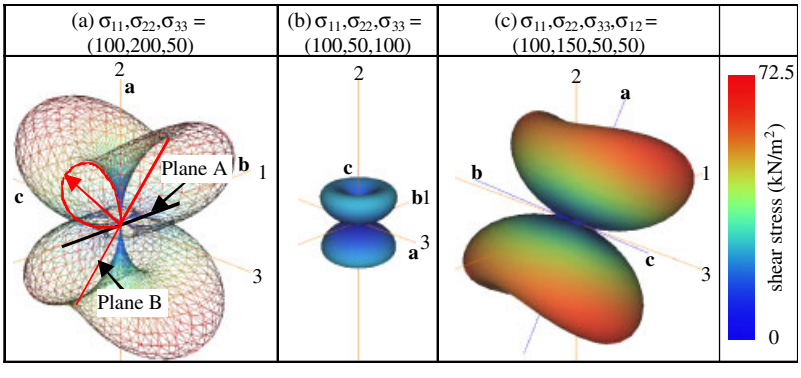

Figure 9. HWY shear stress glyph (stress components not given are equal to zero).

the Mohr circle shown in Figure 8(c). In 3-D, the magnitude of the shear stress gradually decreases in the form of a sinkhole centred on the origin.

The Mohr circle shown in Figure 8(c) does not provide a full three-dimensional representation of the shear stresses. The HWY glyph allows the viewer to see the magnitude of shear stress on any plane in three-dimensional space and provides information complementary to the Reynolds glyph.

Visualization of stress/strain loading histories using hyperstreamlines

Many problems in continuum mechanics emphasize continuous changes in tensor properties [7]. The use of hyperstreamline is extended in this paper to represent changes in stress and strain tensors at a single point. Although glyphs can be animated to display the change of stress/strain state with each load increment, hyperstreamlines offer the viewer the convenience of seeing the loading history at one material point in a single display.

Figure 10 shows the use of a hyperstreamline to visualize the stress history of a uniform triaxial extension test. The hyperstreamline is constructed in 1-2-3 space by consecutively connecting ellipses of intermediate and minor principal stresses and orienting each ellipse based on the direction of the corresponding major principal stress. The ellipse that passes through the origin of the axes system represents the initial state of stress. Subsequent ellipses correspond to states of stress at selected loading increments. The ellipses are connected together by a surface that results in a continuous hyperstreamline propagating in the direction of the major principal stress. The distance between any two ellipses is arbitrarily set as the largest major principal stress

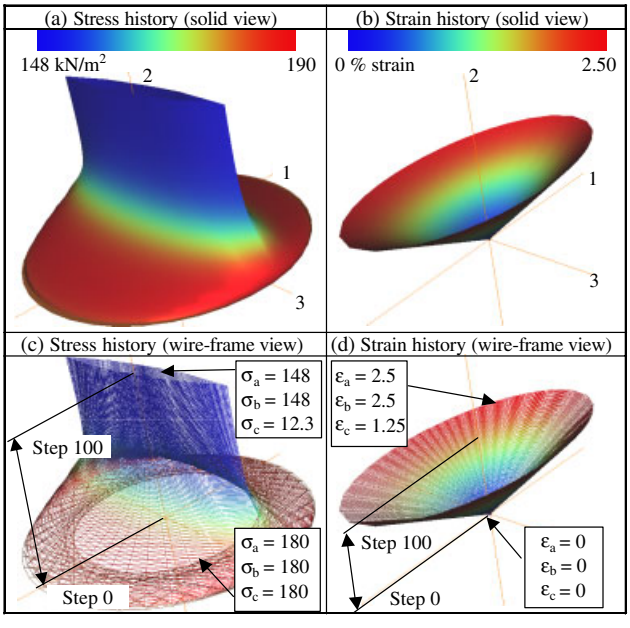

Figure 10. Effective stress and strain hyperstreamline representation of loading history for isotropically consolidated undrained triaxial extension shear test using modified Cam clay model (OCR = 1) with 100 strain steps.

of all loading increments divided by the total number of increments. Magnitude of the major principal stress is indicated by the colour/greyscale on the hyperstreamline. The size of the hyperstreamline cross-section and the rotation about the longitudinal axis of the tube corresponds to the magnitudes and the directions of the intermediate and minor principal stresses, respectively. Each elliptical cross-section shows the stress state corresponding to a given loading (strain) increment. This same procedure can be applied to develop a hyperstreamline to illustrate strain load history shown in Figure 10(b) and (d). The stress and strain hyperstreamlines provide a visual representation of 3-D stress–strain relationship at a single material point.

In the present hyperstreamline representation the signs of the intermediate and minor principal values cannot be visualized. Only the sign and magnitude of the major principal value are mapped in colour or greyscale on the hyperstreamline surface. The stress hyperstreamline maybe considered a stress path plot in 3-D.

IMPLEMENTATION OF GLYPH AND HYPERSTREAMLINE OBJECTS

The glyph and hyperstreamline objects are implemented in VizCoRe [1] and can be used by implemented constitutive models. The objects can be animated to observe changes during a loading sequence. The objects can be examined and rotated in three-dimensional space to examine their features in details. The glyphs though discussed in the context of representing a stress tensor can also be used to represent a strain tensor and are shown in the following examples. The examples only include the use of the Reynolds glyph, the HWY glyph and the step-based hyperstreamline. These objects communicate a richer picture of the stress and strain tensors compared to other glyphs.

APPLICATION TO LABORATORY TRIAXIAL LOADING PATH

The glyphs and hyperstreamlines introduced are used to represent the stress and strain states for simulated laboratory undrained triaxial compression tests using the von Mises [11,12] and the modified Cam clay (MCC [13]) soil models. In principal stress space, the von Mises yield surface takes the form of a cylinder. It is a simple linear elastic perfectly plastic model that is independent of the soil confining pressure. Relevant features of the MCC model include: (1) ellipsoidal isotropic hardening yield surface in principal stress space with an associated flow rule, and (2) critical state defined by a cone in principal stress space whose axis is coincident with the mean stress axis. The two models are used to illustrate how the viewer can observe the differences in the response of the models through visual glyph and hyperstreamline representation.

The tests are summarized in Table II. All the tests are strain driven and have identical states of strains at all loading stages. Figure 11 shows glyph representation of strain tensor used in all the tests. The glyphs for the initial state of strain are nill as no straining has occurred. The glyphs grow as strains increase. The tensile strains in the lateral directions (ε_{11} and ε_{33}) cause a torus-like shape to form around the mid-section of the Reynolds glyph (Figure 11(b),(c)). The increasingly negative lateral strains cause the mid section of the glyph to invert and form the

Table II. Model properties, model state variables, and strain increments for isotropically consolidated undrained triaxial compression shear test (CIUC).

Material Model	Initial state of stress kN/m^2 $[\sigma_{11}, \sigma_{22}, \sigma_{33}, \sigma_{12}, \sigma_{23}, \sigma_{13}]$	Strain increment % $[\Delta\varepsilon_{11}, \Delta\varepsilon_{22}, \Delta\varepsilon_{33}, \Delta\varepsilon_{12}, \Delta\varepsilon_{23}, \Delta\varepsilon_{13}]$	No. of strain increments	Model properties	Model state variables
Test 1 von Mises	[180, 180, 180, 0, 0, 0]	[−0.025, 0.05, −0.025, 0, 0, 0]	98	$E = 7600$ kN/m^2 units, $v = 0.3$, $k = 86.6$ kN/m^2 undrained shear strength of soil	None
Test 2 MCC, OCR = 1.0	[180, 180, 180, 0, 0, 0]	[−0.025, 0.05, −0.025, 0, 0, 0]	98	$\lambda = 0.184$, $\varphi' = 33$, $\kappa = 0.034$, 2G/K = 0.9231	$\alpha = 90$, e = 1.12
Test 3 MCC, OCR = 2.3	[78.7, 78.7, 78.7, 0, 0, 0]	[−0.025, 0.05, −0.025, 0, 0, 0]	98	$\lambda = 0.184$, $\varphi' = 33$, $\kappa = 0.034$, 2G/K = 0.9231	$\alpha = 90$, e = 1.12

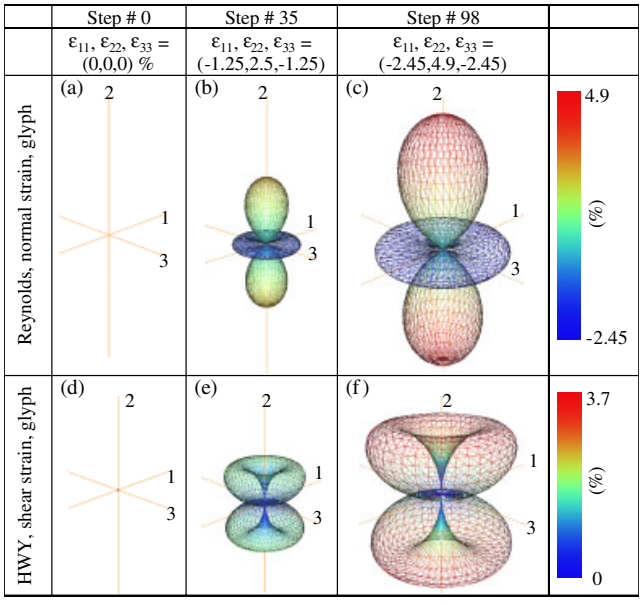

Figure 11. Strain glyph representation for isotropically consolidated undrained triaxial compression shear test (CIUC, all tests, strain components not given are equal to zero).

shape shown. If the lateral strains were positive (compressive), the shape of the Reynolds glyph would be similar to the stress glyph in Figure 7.

Tests 1 and 2 start from the same initial isotropic state of stress using equivalent Boston blue clay properties. The initial state of stress for Test 3 is adjusted to simulate overconsolidated behaviour in the modified Cam clay model. The virtual soil samples are strained incrementally until the specified total number of strain steps is reached. The total number of strain steps is selected such that all the samples reach the failure state and experience equal number of load steps. All stress related plots represent effective stresses.

Figure 12 shows glyph representation of the states of stress for selected strain steps from Test 1. The Reynolds glyph sequence displays the loading process. Initially, Figure 12(a), the glyph is a sphere corresponding to an isotropic state of stress. As compressive vertical strains (ε_{22}) are induced in the vertical direction, the glyph in Figure 12(b) grows vertically and narrows in the 1–3 plane reflecting the normal effective stress increase in the vertical direction and decrease in the lateral direction. The glyph is axisymmetric since the lateral stresses (σ_{11} and σ_{33}) are the same. Once failure is reached, Figure 12(b), the stress does not increase upon further straining, Figure 12(c).

The HWY glyph, used to represent shear stress in any direction is a point under an isotropic state of stress, Figure 12(d). The glyph becomes visible and larger as loading proceeds, Figure 12(e). The maximum shear stress occurs on the 45° planes. The glyph is axisymmetric since the lateral stresses (σ_{11} and σ_{33}) are the same. The shear stress does not increase once failure is reached, Figure 12(f).

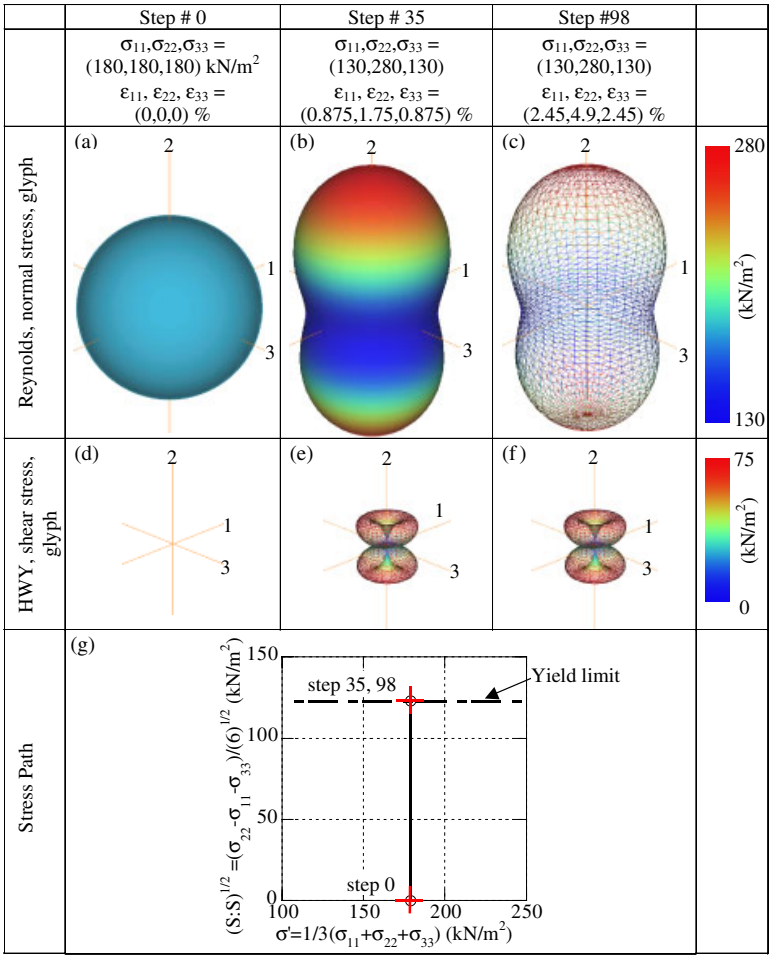

Figure 12. Effective stress glyph representation for CIUC shear test using von Mises model, Test #1 (stress and strain components not given are equal to zero).

The hyperstreamlines for stress and strain history of Test 1 are shown in Figure 13. The hyperstreamlines propagate vertically, in the directions of the major principal stress and strain. The change in colour/shading along the 2-axis reflects the increase in the magnitudes of major principal stress and strain. The cone-like shape of the strain hyperstreamline effectively communicates to the viewer that the size of the intermediate and minor principal strain-loading increments is constant throughout the entire length of the test. The decrease in the radius of the stress hyperstreamline shows the reduction in the magnitude of the minor and intermediate principal stresses. The size of the cross-section becomes constant once the stress level reaches the yield limit. The hyperstreamlines show the evolution of stress and strain in a single figure.

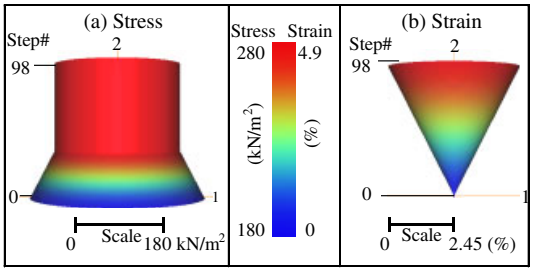

Figure 13. Effective stress and strain hyperstreamline representation for CIUC shear test using von Mises model, Test #1.

Figure 14 shows stress glyph representation of Test 2, which uses the modified Cam clay model with an overconsolidated ratio, OCR = 1. In general, all of the glyphs show similar behaviour compared to those in Figure 12, however the magnitudes of stresses are different. The difference between the two constitutive models is more apparent by examining the stress hyperstreamline, Figure 15. Since the von Mises model is linear elastic prior to reaching the yield limit, the reduction in the radius of the cross-section appears to be linear, Figure 13. On the other hand, the non-linear change in the stress hyperstreamline cross-section for Test 2 is related to the plastic deformation experienced by the normally consolidated MCC soil sample, resulting in a funnel shape. Note that all tests have the same strain hyperstream line.

The results of Test 3 for a slightly overconsolidated sample are displayed in Figure 16. The Reynolds glyph starts as a sphere under the initial isotropic state of stress. The glyph lengthens in the direction of compressive loading and contracts on the plane of the lateral stresses (1–3 plane). The mid-section of the Reynolds glyph starts to grow after step 35 with increasing normal stresses in the lateral directions (σ_{11} and σ_{33}). The HWY glyph shows the continuous increase in shear stresses where it reaches a maximum size at step 35 (Figure 16(e)) and shrinks slightly as it moves toward critical state, Figure 16(f).

The stress hyperstreamline, Figure 17, effectively displays the behaviour experienced in Test 3. The linear decrease in the radius of the cross-section of the tube distinguishes the elastic phase of the loading from the plastic portion. The elastic phase is similar to that in the von-Mises Test 1, Figure 13(a). Once the yield surface is reached, the mean effective stress (σ') increases, and the cross-section of the tube expands, but nonlinearly until the stress state reaches the failure cone.

APPLICATION TO STRESS–STRAIN PATH FROM A BRACED EXCAVATION BOUNDARY VALUE PROBLEM

Hashash [14] performed numerical experiments to understand braced excavation behaviour using the modified Cam clay model with Boston blue clay properties. The geometry of the excavation and the configuration of the bracing and wall are shown in Figure 18. The excavation is performed in 9 stages whereby the soil is excavated in 2.5 m increments and bracing is installed. The analysis assumes plane strain condition. Stress and strain data from the nine stages are extracted from the numerical analysis at point (3C) and are summarized in Table III.

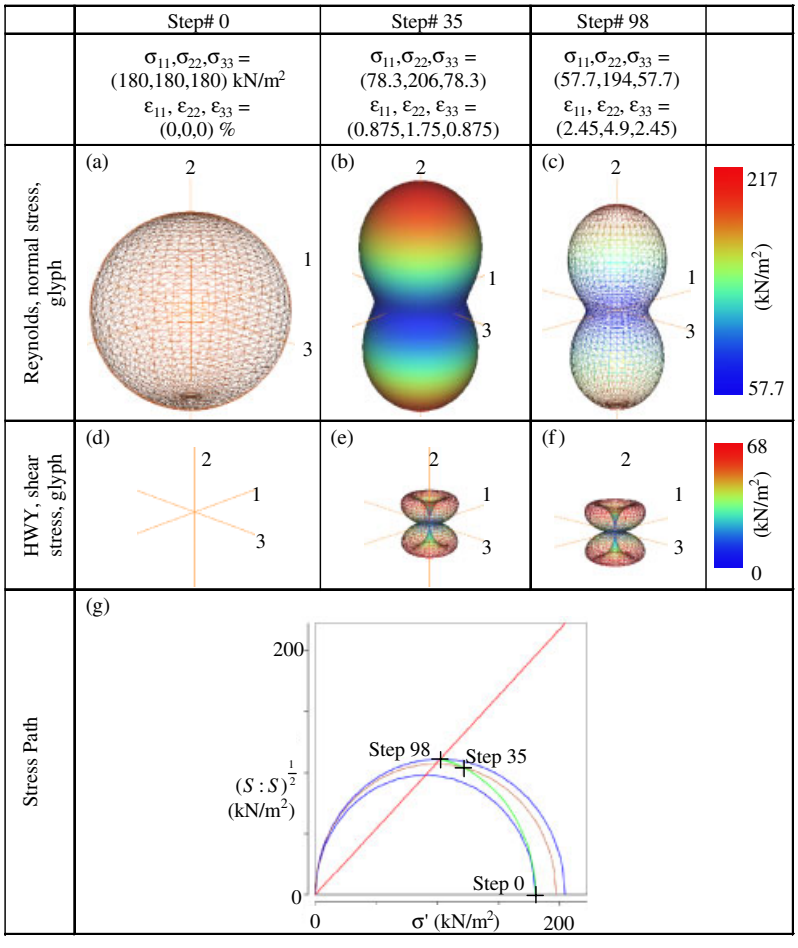

Figure 14. Effective stress glyph representation for CIUC test using modified Cam clay model (OCR = 1, Test #2, stress and strain components not given are equal to zero).

Figure 19 shows glyph representation of the state of strain for selected excavation stages. Prior to the start of excavation no straining has occurred, therefore boxes (Figure 19(a),(d)) for Reynolds and HWY glyphs display nothing. As soil is removed in later stages, Figure 19(b) shows that the Reynolds glyph develops four equal-size lobes. One set of lobes has cooler (darker) colours which indicates tensile strains, while the set with warmer (lighter) colours represents compressive strains. The tensile straining occurs along the minor principal direction (**c**) since the soil excavation causes the wall to move laterally outward resulting in tensile (negative) lateral strains as well as shear strains on vertical planes. The lobes gradually grow in size and rotate counterclockwise in the 1–2 plane. At step 6 (Figure 19(b)) the Reynolds glyph begins to decrease in size and rotates in the reverse direction for steps 8 (not shown) and 9. The glyph clearly illustrates the assumption of plane strain condition because along the 3-axis all the lobes end as a point at the origin corresponding to a zero out-of-plane strain.

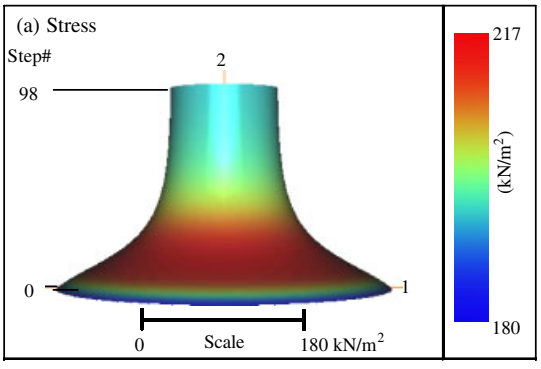

Figure 15. Effective stress hyperstreamline representation for CIUC test using modified Cam clay model (OCR = 1, Test #2).

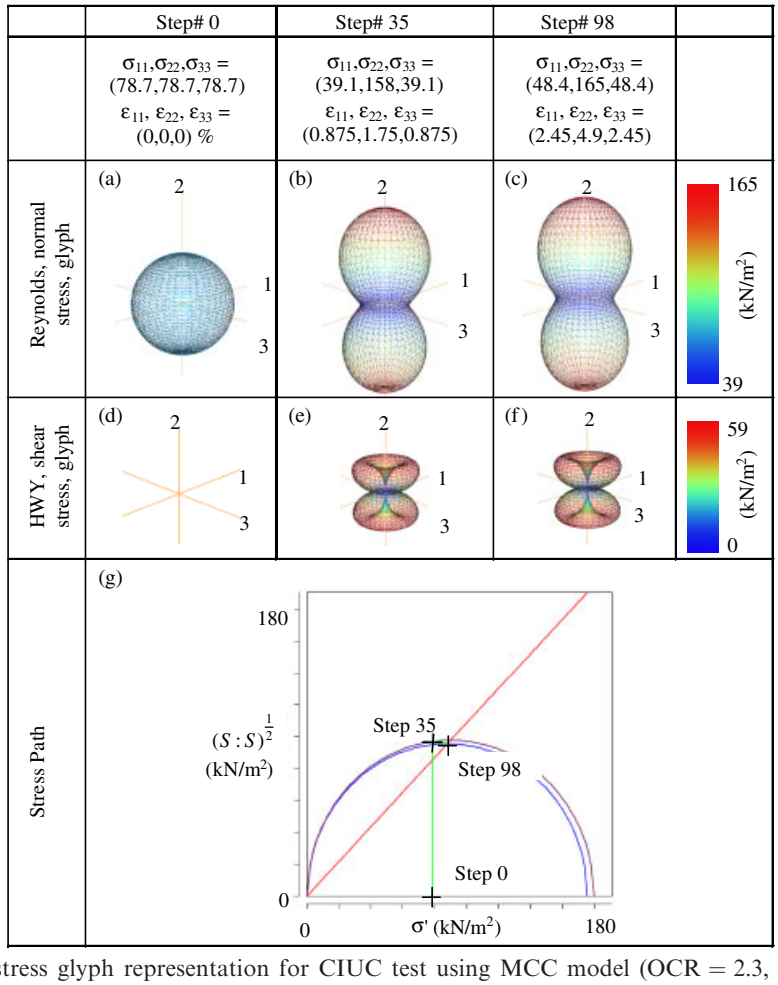

Figure 16. Effective stress glyph representation for CIUC test using MCC model (OCR = 2.3, Test #2, stress and strain components not given are equal to zero).

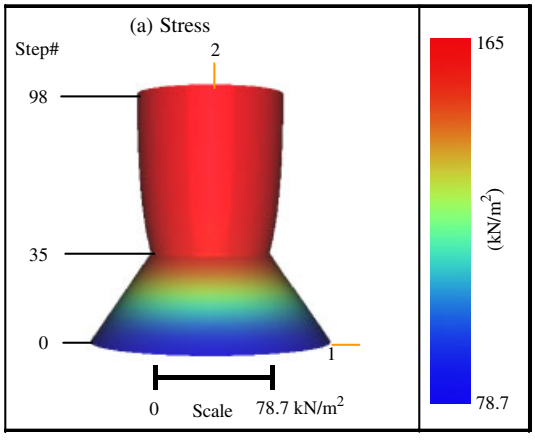

Figure 17. Effective stress hyperstreamline representation for CIUC test using MCC model (OCR = 2.3, Test #2).

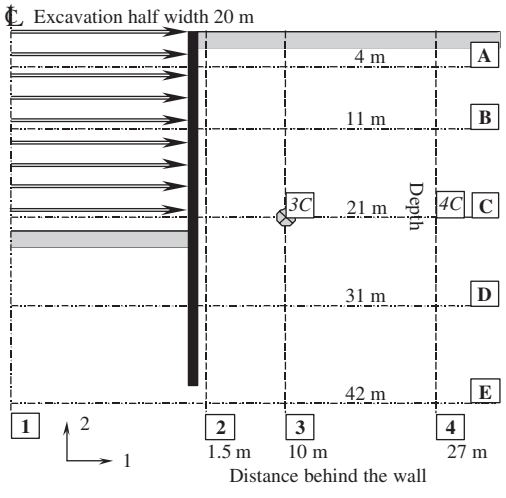

Figure 18. Geometry of braced excavation and location of reference soil element (after Hashash [14]).

The HWY glyph for shear strain representation shows similar pattern of changes in size and rotation of the Reynolds glyph. Initially, the glyph increases in size and rotates counterclockwise in the 1–2 plane. The glyph shows an increase in shear strains. The glyph then decreases in size at step 9, Figure 19(e), and rotates in the reverse direction for the last two stages.

Figure 20 shows glyph representation of the state of stress for selected excavation stages. The Reynolds stress glyph, under the initial $K_0 = 0.5$, has a 'peanut' shape and is oriented along the 1-2-3 axes (Figure 20(a)). As the excavation proceeds, the introduction of shear stresses along vertical planes causes the glyph to rotate off of the 2-axis and shrink along its longitudinal axis until the last step. The middle section of the Reynolds glyph shrinks from step 1–6 in the directions of both minor and intermediate principal stresses. Following step 4 (not shown), the glyph rotates back toward the 2-axis, and beginning at step 6 its middle section swells laterally in the minor principal direction.

Table III. Model properties, model state variables and stress and strain output for Element 3C in Figure 18.

	Stage/excavation depth (m)	Strain increment % $[\varepsilon_{11}, \varepsilon_{22}, \varepsilon_{33}, \varepsilon_{12}, \varepsilon_{23}, \varepsilon_{13}]$	$[\sigma_{11}, \sigma_{22}, \sigma_{33}, \sigma_{12}, \sigma_{23}, \sigma_{13}]$ (kN/m^2)
Material model:	Initial/0	[0.0000, 0.0000, 0, 0.000, 0, 0]	[109, 204, 109, 0, 0, 0]
Modified Cam Clay Model	1/2.5	[−0.0253, 0.0251, 0, 0.183, 0, 0]	[106, 203, 108, 7.56, 0, 0]
(OCR = 1.0)	2/5.0	[−0.0810, 0.0818, 0, 0.279, 0, 0]	[101, 202, 107, 11.0, 0, 0]
	3/7.5	[−0.1340, 0.1350, 0, 0.348, 0, 0]	[95.7, 201, 106, 13.3, 0, 0]
Model properties:	4/10.0	[−0.1780, 0.1800, 0, 0.389, 0, 0]	[91.8, 200, 105, 14.3, 0, 0]
$\lambda = 0.184$, $\varphi' = 33.4$,	5/12.5	[−0.2090, 0.2100, 0, 0.402, 0, 0]	[89.2, 200, 105, 14.5, 0, 0]
$\kappa = 0.034$,			
2G/K = 1.05	6/15.0	[−0.2210, 0.2220, 0, 0.387, 0, 0]	[88.2, 200, 104, 13.8, 0, 0]
	7/17.5	[−0.2150, 0.2150, 0, 0.356, 0, 0]	[88.7, 199, 104, 12.6, 0, 0]
Model state variables:	8/20.0	[−0.1930, 0.1930, 0, 0.322, 0, 0]	[90.4, 197, 104, 11.3, 0, 0]
$\alpha = 87.94$, e = 0.957	9/22.5	[−0.1590, 0.1590, 0, 0.296, 0, 0]	[93.1, 195, 104, 10.2, 0, 0]

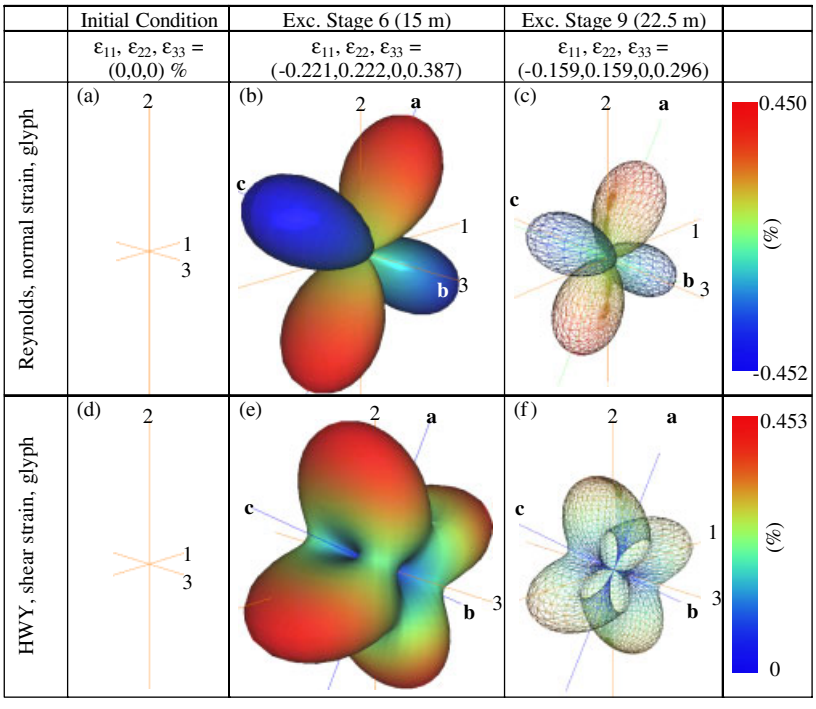

Figure 19. Strain glyph representation of the loading of a soil element behind an excavation using MCC soil model (strain components not given are equal to zero).

The HWY glyph exhibits similar behaviour starting off with axisymmetric shape along the 1-2-3 axes, Figure 20(d). The glyph rotates off of the 2-axis and gradually inflates. The geometry also becomes asymmetrical due to prevailing plane strain conditions. After step 6, the glyph rotates back toward the 2-axis and shrinks as shear stresses reduce.

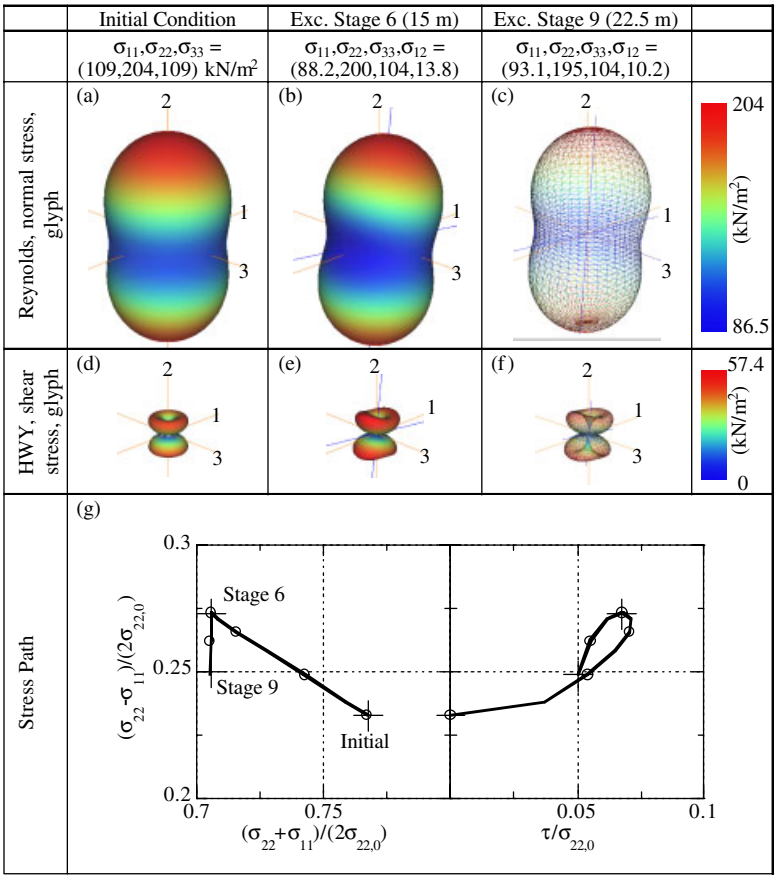

Figure 20. Effective stress glyph representation of the loading of a soil element behind an excavation using MCC soil model (stress components not given are equal to zero).

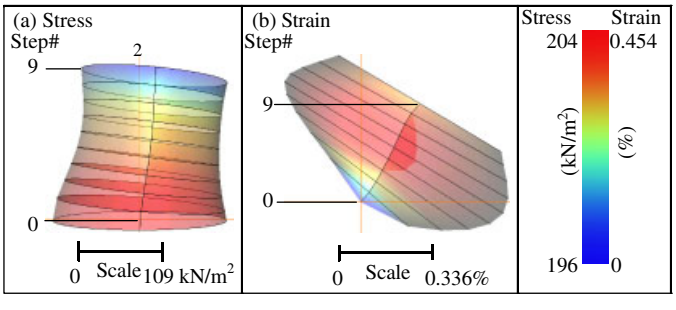

Figure 21. Effective stress and strain hyperstreamline representation of the loading of a soil element behind an excavation using MCC soil model.

Figure 21 shows the hyperstreamline representation of the stress and strain history at point (3C). Wire-frame view is used to better illustrate the change in geometry. Hyperstreamline

representation of the strain history is a plane surface because the out of plane strain is zero under plane strain conditions. The change in the magnitude and direction of the major principal stress is clearly presented by the colour and shape of the tube respectively. The stress hyperstreamline shows similar features to glyphs of Figure 20 in a single display, namely (1) rotation of major principal stress direction away from the 2-axis for steps 1–4, (2) decrease in major principal stress for steps 1–9, (3) rotation of major principal stress direction toward the 2-axis for steps 5–9, and (4) the initial decrease and subsequent increase in magnitude of minor principal stress.

CONCLUSIONS

This paper develops glyphs and hyperstreamlines for visualization of stress and strain tensors. The HWY glyph is introduced to represent shear stresses. A hyperstreamline is developed to show the evolution of stress and strain tensors during general shearing. These visual objects provide a greater understanding of the complex loading that the soil undergoes in the analysis of a boundary value problem. These objects provide an important link to understanding the role of a constitutive model in these complex shearing modes. The development is made using the VizCoRe platform and can be accessed at http://www.cee.uiuc.edu/VizCoRe.

ACKNOWLEDGEMENTS

This material is based upon work supported in part by the National Science Foundation under Grant No. 9984125. Any opinions, findings, and conclusions or recommendations expressed in this material are those of the authors and do not necessarily reflect the views of the National Science Foundation.

VizCoRe uses VisAD, a Java component library for interactive and collaborative visualization and analysis of numerical data as part of the graphics renderer. The authors would like to acknowledge the University Corporation for Atmospheric Research (UCAR)/Unidata and Bill Hibbard, the VisAD development group and community for their assistance in use of VizAD.

REFERENCES

1. Hashash YMA, Wotring D, Yao JI-C, Lee J-S, Fu Q. Visual framework for development and use of constitutive models. *International Journal for Numerical and Analytical Methods in Geomechanics* 2002; **26**:1493–1513.
2. Haber RB. Visualization techniques for engineering mechanics. *Computing Systems in Engineering* 1990; **1**(1):37–50.
3. Delmarcelle T. The visualization of second-order tensor fields. *Ph.D*. In Applied Physics. Stanford University, 1994; 204.
4. Delmarcelle T, Hesselink L. Visualization of second-order tensor fields and matrix data. In *Proceedings of IEEE Visualization Conference '91*. IEEE Computer Society Press: Los Alamitos, CA, 1992; 316–323.
5. Jeremic B, Scheuermann G, Frey J, Yang Z, Hamann B, Joy KI, Hagen H. Tensor visualizations in computational geomechanics. *International Journal for Numerical and Analytical Methods in Geomechanics* 2001; **01**(1-6).
6. Frederick D, Chang TS. *Continuum Mechanics*. Allyn and Bacon, Inc.: Boston, 1965; 218.
7. Kriz RD, Glaessen EH, MacRae JD. Eigenvalue-Eigenvector glyphs: Visualizing zeroth, second, fourth and higher order tensors in a continuum. In *Workshop on Modeling the Development of Residual Stresses During Thermoset Composite Curing*. University of Illinois: Champaign-Urbana, 1995.
8. Helman JL, Hesselink L. Visualizing vector field topology in fluid flows. *IEEE Computer Graphics & Applications* 1991; **11**(3):36–46.
9. Fung YC. *Foundations of solid mechanics*. Prentice-Hall international series in dynamics: Englewood Cliffs, NJ, 1965; 525.
10. Moore JG, Schorn SA, Moore J. Methods of classical mechanics applied to turbulence stresses in a tip leakage vortex. In *International Gas Turbine and Aeroengine Congress & Exposition*. AMSE: Houston, TX, 1995; 11.

11. Hill R. *The Mathematical Theory of Plasticity*. *Oxford Engineering Science Series*, Clarendon Press: Oxford, vol. IX. 1950; 356.
12. Boresi AP, Schmidt RJ, Sidebottom OM. *Advanced Mechanics of Materials* (5th edn). John Wiley & Sons Inc.: New York, 1993; 811.
13. Roscoe KH, Burland JB. On the generalized stress–strain behaviour of 'wet' clay. In *Engineering Plasticity*, Heyman J (ed.). Cambridge University Press: Cambridge, England, 1968; 535–609.
14. Hashash YMA. Analysis of deep excavations in clay. *Ph.D*. In Department of Civil and Environmental Engineering. Massatchusetts Institute of Technology: Cambridge: 1992; 337.

